J. Membrane Biol. 74, 229–245 (1983)

The Journal of
Membrane Biology

Potential Dependence of the Admittance of *Chara* Plasmalemma

M.J. Beilby and B.N. Beilby
Botany School, University of Cambridge, Cambridge CB2 3EA, England

Summary. A computer-controlled apparatus is described, which combines the two powerful methods of voltage-clamping and admittance measurement. The 5-Hz admittance of *Chara* plasmalemma is obtained for transmembrane PD from −400 mV to 0. DC conductance is also measured by the bipolar staircase method. Both the DC and 5-Hz conductances at steady state display a central maximum at ~ −250 mV. This feature is attributed to the conductance/voltage characteristics of the H^+ pump. The steady-state capacitance does not show any trend throughout the potential interval.

At the time of the delay, before excitation commences, the 5-Hz conductance is smaller than after excitation.

At the time of excitation the 5-Hz conductance echoes the time-course of the ionic current, while the capacitance undergoes a sharp decrease followed by an increase. A possible explanation of the capacitance behavior is attempted involving transport number effects and reactances associated with the Hodgkin-Huxley gating mechanism.

At punchthrough the membrane becomes inductive.

Key Words *Chara* · voltage clamp · admittance · proton pump · action potential · punchthrough · transport number effects

Introduction

In previous experiments the membrane conductance G was usually measured by superimposing a small perturbation waveform on to the clamp commands or the current passed through the membrane (e.g., Findlay & Hope, 1964; Shimmen & Tazawa, 1980; Beilby, 1981). G was calculated as I_o/V_o (where I_o and V_o are the amplitudes of the current and potential waveforms, respectively). The well-documented membrane reactance (e.g., Curtis & Cole, 1937; Coster & Smith, 1977), which requires a measurement of phase angle ϕ between the perturbation and response waveforms, was neglected. One reason for this omission is the tedium and inefficiency of the AC bridge method usually employed (e.g., Cole & Curtis, 1939; Kishimoto, 1974). This particularly applies to fast events, such as excitation. Fortunately, the advent of small computers offers a new approach to ϕ measurement (e.g., Bell, Coster & Smith, 1975). This communication describes a simple voltage-clamp circuit with computer-controlled commands and data acquisition. The increased accuracy, better data accessibility and versatility of the clamp commands make the measurement of the membrane admittance more feasible. (Admittance, rather than impedance, is mathematically more convenient to express the conventional model of the membrane as the combination in parallel of resistance R and capacitance C.) The method of using time-varying command potentials for voltage clamping is similar to that utilized by Palti and Adelman (1969) for the squid axon.

The historical measurements that produced the value of capacitance in biological membranes (Cole & Curtis, 1939; Cole, 1968) also established the doctrine of its invariance. The Hodgkin-Huxley (HH) equations have been formulated with this view in mind (Hodgkin & Huxley, 1952). It is now known, however, that reactive components of the impedance arise from the time-dependent ionic currents (e.g., Chandler, Fitz Hugh & Cole, 1962) and from the movement of the gating particles (e.g., Armstrong & Bezanilla, 1973; Keynes & Rojas, 1974). These capacitances and inductances have relatively long time constants and can be detected only at low frequencies (<1 kHz). The behavior of the reactance at different clamp PDs and at the time of excitation may thus provide information about the changes in the membrane structure under various conditions.

Measurements of admittance Y and phase angle ϕ (and resultant G and C) of *Chara* plasmalemma at 5 Hz and clamp levels between −400 mV and 0 are presented here.

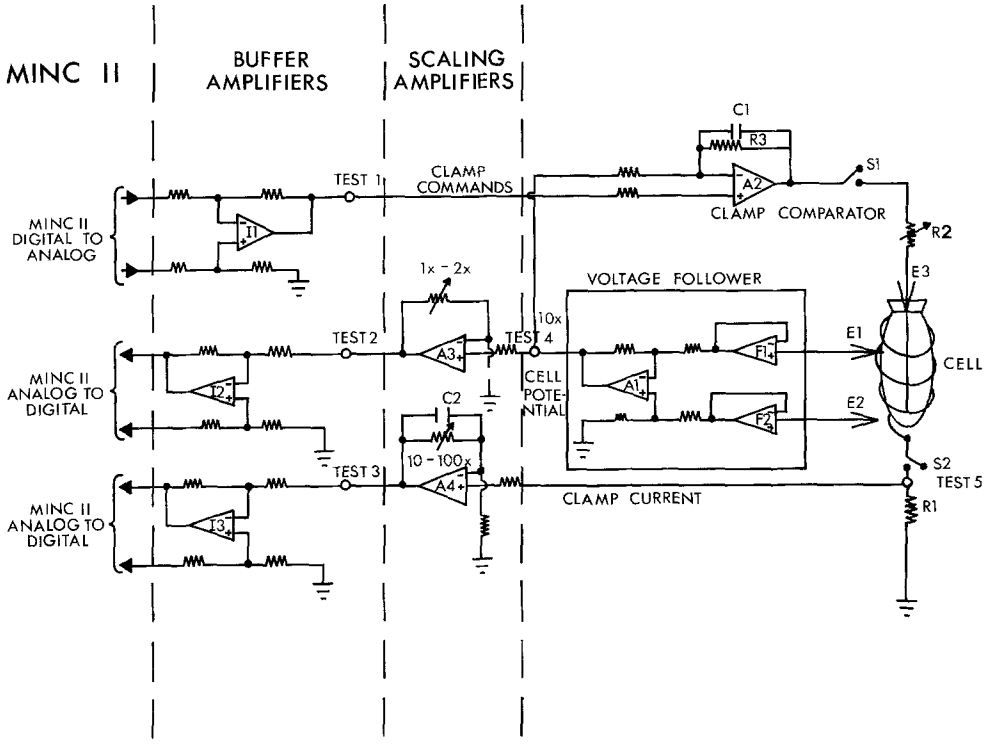

Fig. 1. The experimental apparatus. The clamp comparator (*A2*) consists of the operational amplifier 741, with the values of *C1* and *R3* adjusted to prevent high frequency oscillations. The voltage follower utilizes bipolar operational amplifiers (*F1* and *F2*) with long-tailed pair of field effect transistors at their inputs. These are placed adjacent to the potential-measuring electrodes *E1* and *E2*. Such an arrangement reduces the transmission distance of the high impedance signal and minimizes noise pick-up. The connections between the microelectrodes and the circuitry are provided by Ag/AgCl half cells (WPI). *E1* and *E2* are glass micropipettes filled with 2 M KCl ("Kwik-fil" single capillaries with inner filament, 2 mm OD, Clark Electromedical Instruments). To enter the cytoplasm easily the microelectrode *E1* was pulled with a broad taper. The current-injecting electrode *E3* is Pt/Ir wire etched in KCN solution from 50 to ~5 μm diameter. The wire is manipulated into the cell through a glass micropipette which has been broken back. To obtain maximum resolution from the digitizing process, the measured potentials were adjusted for the ±5.12 V A/D by the scaling amplifiers (*A3* and *A4*). To avoid earth loops between the computer and the clamp circuitry differential amplifiers (*I1*, *I2* and *I3*) are used. The clamp commands are provided by the computer D/A with voltage range chosen as ±5.12 V. A dual trace oscilloscope was included in the circuit at the point *TEST2* to ensure the optimum conditions. *TEST1* was also monitored to check the command potential. To provide a real-time view of the progress of the experiment a chart recorder was connected to the points *TEST2* and *TEST3*

Materials and Methods

Hardware

The experimental set-up is described in Fig. 1. The right-hand side of the circuit was already outlined by Beilby (1981). More details are added here as they become relevant in the present context. The voltage follower was designed by Mr. P. Joyce, Physiological Laboratory, University of Cambridge. The use of the longitudinal current electrode E3 was necessary to provide a uniform current density, to avoid propagation of excitation along the length of the cell, and to average the cell conductance. The last aspect became particularly important in the light of the recent finding that the acid and alkaline bands (Spear, Barr & Barr, 1969) correspond to regions of varying conductance (e.g., Walker, 1982)[1].

The MINC 11 computer was obtained from Digital Equipment Co., Ltd. (DEC). The configuration consisted of LSI 11/03 central processor, 32 K words of memory, RX02 dual disk drive, VT105 video terminal, LA34 Decwriter printer, MNCAD single 12-bit analog-to-digital converter (A/D) with 16 multiplexer inputs, MNCAA 12-bit digital-to-analog converter (D/A) and MNKWC clock module. A hard copy of the graphs was provided by digital plotter Watanabe WX4671.

Software

The software provided by DEC to drive the A/D and D/A converters was unsuitable for our experiments and our own subroutines were written in MACRO (DEC assembly machine language). The bulk of our programming was done in FORTRAN.

The task of measurements and data analysis was divided among several programs. At present three types of clamp commands have been developed:

1) The first type of command, generated by program COMSET, clamped the membrane PD at the resting potential for 1.0 sec, then to a desired level. The cell was returned to the resting potential 2.0 sec prior to the end of the clamp. An

[1] Chilcott, T.C., Coster, H.G.L., Ogata, K., Smith, J.R. Spatial variation of the electrical properties of *Chara*: II. Membrane capacitance and conductance as a function of frequency. (*In preparation.*)

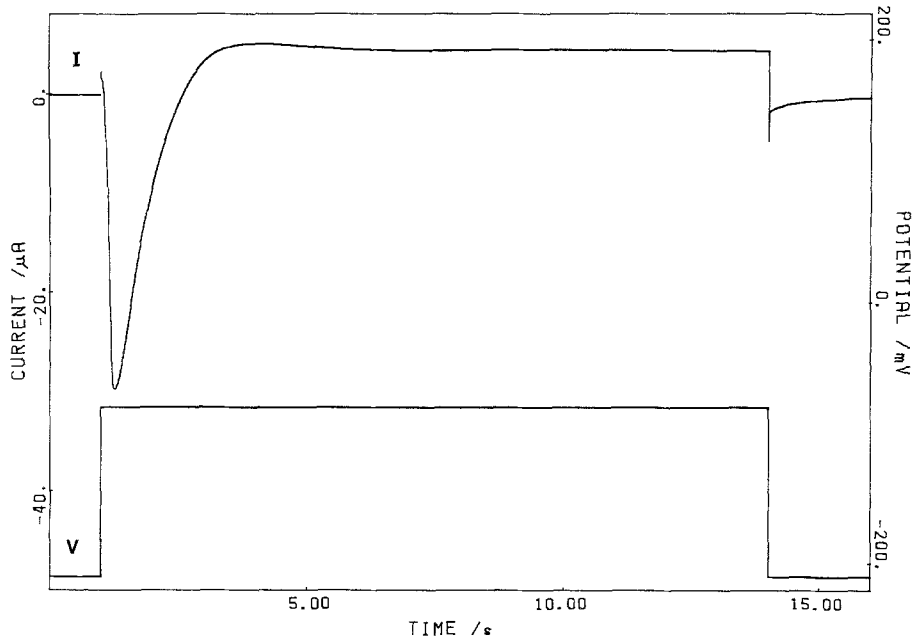

Fig. 2. An example of the basic clamp command: cell is clamped to the resting potential for 1.0 sec, then to −80 mV for 13 sec and finally to the resting potential again (lower trace). The current response of the cell, measured across resistor *R*1, is shown as the upper trace. The cell area was 17 mm^2

example of such a command sequence is shown in Fig. 2. The command array was stored on disk as COMAND file. COMSET also kept track of the experimental conditions. Since experiments tend to be repetitive, time was saved by displaying a menu on the screen (*see* Table). The information displayed by the menu was also stored in the COMAND file.

2) Second command program, VISET, provided a bipolar staircase to obtain the voltage-current (*V*/*I*) characteristics of the membrane (e.g., Walker, Beilby & Smith, 1979). An example is shown in Fig. 3. Similar to COMSET, this program generated a menu and a COMAND file.

3) Program COMSET also generated the third type of clamp command by superimposing a sine wave of 5 Hz on to the commands of (1) to measure the admittance at different clamp potentials. The amplitude of the sine wave could be chosen by the menu program (*see* Table). Amplitudes between 10 and 40 mV were usually selected, depending on the clamp level and the cell conductance. (The amplitude of the applied sine wave had to be large enough so that the current response was distinguishable from the instrumentation noise.) The frequency was chosen as a compromise: it had to be sufficiently low to reflect the AC conductance of the membrane (Coster & Smith, 1977; Smith & Coster, 1980), yet high enough to permit rapid measurement of the *G* and *C*. In future work the apparatus will be able to explore the the frequency range up to 100 Hz. To measure the admittance accurately, a smooth sine wave was necessary. The calibration procedures established that 800 points per sine cycle (at 5 Hz) was satisfactory. For an example of commands of this type *see* Fig. 4*a*.

Having defined the clamp commands the programs IMPLOG (COMSET commands) or VIRUN (VISET commands) were called. These programs read the COMAND file and performed the measurements. Their size was kept to a minimum to optimize the memory space available for the data. One current point and one potential point A/D conversion was done every 2 msec (giving 100 points for each current and potential sine cycle). At this rate the memory was filled in 16 sec. At the end of the clamp run the data file was created on disk. The name of each data file contained the cell number and the run number (*see* Table).

After the clamp run program REGURG displayed the data on the screen in the terms of the A/D potential against time. This program would also "blow up" a selected portion of the graph. A hard copy was provided by program FREEZE on the Watanabe WX4671 digital plotter. The A/D voltages were converted into μA and mV. Examples of such output are shown in Figs. 2, 3 and 4.

A special version of command (3) was furnished by program SINUS for admittance measurement at potentials where the membrane behavior was time-invariant (−150 to −350 mV). The membrane was clamped to a selected level for 4.0 sec only. SINUS also performed the measurements and subsequent analysis providing a fast measurement of *G* and *C*.

Experimental Procedure

A young leaf cell of *Chara corallina* was placed in the coil and the longitudinal electrode inserted. Standard APW (NaCl, 1.0 mM; KCl, 0.1 mM; $CaCl_2$, 0.5 mM; HEPES, 1.0 mM; NaOH to adjust to pH 7.5, 0.47 mM) was used. Before the potential-measuring microelectrodes were connected, a known *RC* combination was measured with program SINUS to check the calibration of the apparatus. About half an hour after the insertion of the wire (*E*3, *see* Fig. 1), the side electrodes (*E*1 and *E*2) were manipulated close the the cell. The program COMSET was called. The cell dimensions were estimated with a graticule, and the menu was updated. Before inserting *E*1 into the cytoplasm the electrode offset PD was measured. Electrodes with an offset >10 mV were discarded. The cytoplasmic electrode was then inserted and the COMAND file prepared. Program IMPLOG was called to perform the measurement, and REGURG displayed the data.

The first clamp level for each cell was at 0. At this potential the clamp current across plasmalemma shows a prominent positive peak not observed if *E*1 is in the vacuole (Beilby & Coster, 1979*a*). The position of the inside electrode was thus ascertained.

The sequence of COMSET, IMPLOG, and REGURG took about 5 min, the longest time being the transfer of arrays from and onto disk.

Table. Program COMSET – sampling parameters at 13:04:30 on 31 May 82

1. Cell number 17 Area 0.1751E-04 m-sq
2. Electrode offset −0.66 (0.05) mV
3. Run number 4
4. Solution CL APW, DIM LIGHT
5. pH 7.50
6. Temperature 23.70 deg C
7. Clamp level −80 mV
8. Sine amplitude 0 mV
9. Current Amplifier Scale 10 −45.29 μA 0.022402 μA/div
10. Voltage amplifier scale 1 −252.37 mV 0.123222 mV/div
11. D/A Driving Rate 250 μs
    A/D Sampling Rate 2.000 ms
12. Steps/cycle 100
    Frequency 5.00 Hz
13. Run-in Time 1000 samples (2.000 sec 10.000 cycles)
14. Clamp ON at 500 samples (1.000 sec 5.000 cycles)
15. Clamp OFF at 7000 samples (14.000 sec 70.000 cycles)
16. Total Run Time 8000 samples (16.000 sec 80.000 cycles)
    Resting potential −210.06 (0.05) mV
    Sine Curve D/A Values
    0.00 2365.43 2881.42 800 Points
    Data File is C00017.R04

A menu generated by the program COMSET. (The resultant clamp run is shown in Fig. 2). The menu appears on the screen as COMSET is called and can be updated by typing the appropriate number on the left-hand side and entering the new information in. Number "2" initiates 100 potential measurements by the channel 6 of the A/D. "7" and "8" control the clamp commands. "9" and "10" perform recalibration. "11" and "12" control the frequency and sampling rate. (The values displayed remained constant throughout all experiments described.)

"13" determines how long the D/A is "run in" to ensure a steady command potential. "14" to "16" set the run time and how long the cells is clamped to resting potential at the beginning and end. The menu is echoed by the printer as COMSET is exited. To do so "17" is called (not reproduced by the printer). This number also initiates the resting potential measurement.

Data Analysis and Numerical Methods

V/I Curves. Program VIPLOT analyzed the data collected by the VISET/VIRUN sequence (*see* Fig. 3). Figure 3*b* shows that the clamp potential pulse (lower trace) was well-shaped and the rise time was completed in 4.0 msec (data-logging rate was 2 msec/sample, shown by the points). The spikes accompanying the current pulses (upper trace) were generated by the comparator "hitting the rails" to produce the largest possible current output, so that the cell PD could be driven to the command PD speedily and efficiently. These current surges lasted only several msec and did not seem detrimental to the cell. The staircase clamp could be repeated many times without affecting the resting potential or the cytoplasmic streaming.

Before settling to a steady value the initial time-course of the current pulse was determined by the *RC* characteristics of the cell and the AC characteristics of the comparator. Some adjustment could be made by varying the capacitor *C*1 and the resistor *R*2 (*see* Fig. 1). After the initial spike the clamp current pulse stabilized to a steady value (*see* arrows on Fig. 3*b*), which was plotted against the clamp PD by VIPLOT (*see* Fig. 9*a*). For most cells, pulses wider than 20 msec were necessary to obtain a current plateau.

The *V/I* curves could be satisfactorily fitted with polynomials of degree less than 10. The method of least squares was employed to determine the best fit. The polynomial was differentiated at chosen points of the *V/I* curve yielding the slope conductance as a function of the membrane potential (*see* Fig. 9*b*).

Admittance Measurements. This analysis involves the amplitude and phase of the alternating current response rather than the ionic current baselines. The time-varying part of the clamp potential can be expressed as:

$$\tilde{V} = V_o e^{j\omega t} \tag{1}$$

V_o = potential sinewave amplitude

t = time

$j = \sqrt{-1}$

$\omega = 2\pi f$, where f = frequency of 5 Hz.

The alternating current response is displaced by a phase angle ϕ due to the membrane reactance:

$$\tilde{I} = I_o e^{j(\omega t + \phi)}. \tag{2}$$

From Ohm's Law:

$$\tilde{I} = \tilde{Y}\tilde{V} \tag{3}$$

$$\tilde{Y} = G + j\,\omega\, C. \tag{4}$$

Combined Eqs. (1) to (4) yield:

$$Y_o = I_o/V_o = \sqrt{G^2 + (\omega C)^2} \tag{5a}$$

$$\phi = \arctan(\omega C/G). \tag{5b}$$

Rearranging Eqs. (5a) and (5b):

$$G = (I_o/V_o)\cos\phi \tag{6}$$

$$C = (I_o/V_o\,\omega)\sin\phi. \tag{7}$$

V_o and ω were selected, I_o and ϕ were measured.

The first step in the evaluation of I_o and ϕ was the stripping of the ionic current baseline. This procedure was performed by the program STRIP. To calculate the baseline from data such as Fig. 4*a*, a point on the current trace was considered as a midpoint of a single sine cycle. The average value of the total current over that cycle was found. The program then advanced by one data point and the calculation was repeated. The baseline for the first and the last fifty points in the current array was obtained by extrapolation. Similarly, half a cycle before and after the clamp level changes (*see* shaded portions of Fig. 4*b* to *d*) the baseline was extrapolated. Thus the results in these regions give only approximate values. The stripping process was repeated for the clamp potential array, mainly to ascertain that the program was working reliably. The current baseline and sine wave can be seen in Fig. 4*b*. After the baselines were subtracted from the total current and potential arrays, the sine waves became available for the I_o and ϕ calculation. The admittance amplitude $Y_o\,(=I_o/V_o)$ and the phase angle ϕ are shown in Fig. 4*c*. G and C were calculated from Eqs (6) and (7) and are displayed in Fig. 4*d*.

A special version of the STRIP program was used to calculate the steady state G and C. This program (called EXAMIT) analyzed the first four cycles (cell clamped at the resting potential), the last five cycles before the clamp level change back to resting potential, and the four cycles at the resting potential at the end of the run.

The subtracted current baseline was compared with unmodulated clamp runs at the same potential level (Fig. 5). The

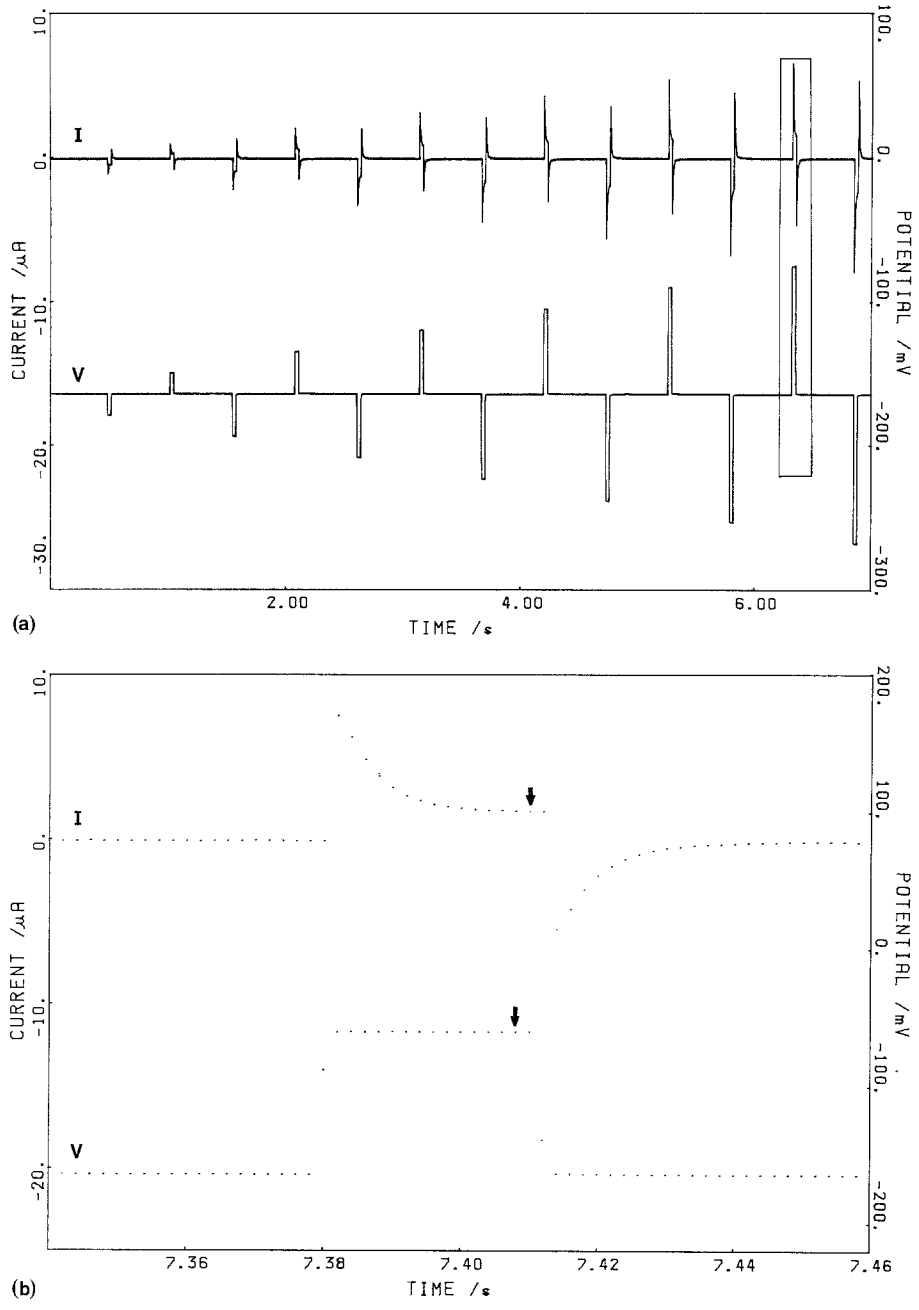

Fig. 3. *(a)* A bipolar staircase clamp command generated by program VISET: clamp potential (lower trace), clamp current (upper trace). The rate of increase, the pulse width, and the pulse spacing can be selected with a menu similar to that of COMSET. The area delimited by the rectangle on the right is enlarged in *b*. *(b)*: The points represent samples of clamp potential and current taken by the A/D. The arrows indicate the points used by VIPLOT to construct a V/I curve. The cell area was 17 mm^2

baseline showed some deviation within the first two cycles, particularly the extrapolated half-cycle. These difficulties were most severe at clamp levels with prompt currents, such as −80 mV (Fig. 5) or 0. The fitting procedure worked most reliably near threshold, where the currents changed slowly. The threshold potential became more negative, however, with the superimposed sinewave.

Some clamp current baselines at the time of excitation showed a slight modulation of the same frequency as the perturbation waveform (*see*, for instance, Fig. 5). As this effect was never observed in the clamp potential baseline, it seems unlikely that it is an artifact of the stripping process. The modulation probably occurred due to the voltage-dependence of the Hodgkin-Huxley (HH) parameters (Beilby & Coster, 1979*b*).

Calibration and Accuracy

Both the D/A and the A/D have been set on the voltage range of ±5.12 V, giving single bit resolution of 2.5 mV or 0.03%. In our calibration experiments we found that even when measuring test voltages internal to the computer two bits were drowned by noise. In the experimental measurements the noise usually spanned two to three bits.

The clamp potential and current were recorded by the A/D channels as potentials adjusted by the scaling and buffer amplifiers. For an accurate measurement, the amplification factors and the null offsets for all the amplifier stages must be known.

To calibrate the clamp potential arm of the circuit (i.e., *I*1, *A*3 and *I*2, see Fig. 1) a Solatron digital voltmeter was at-

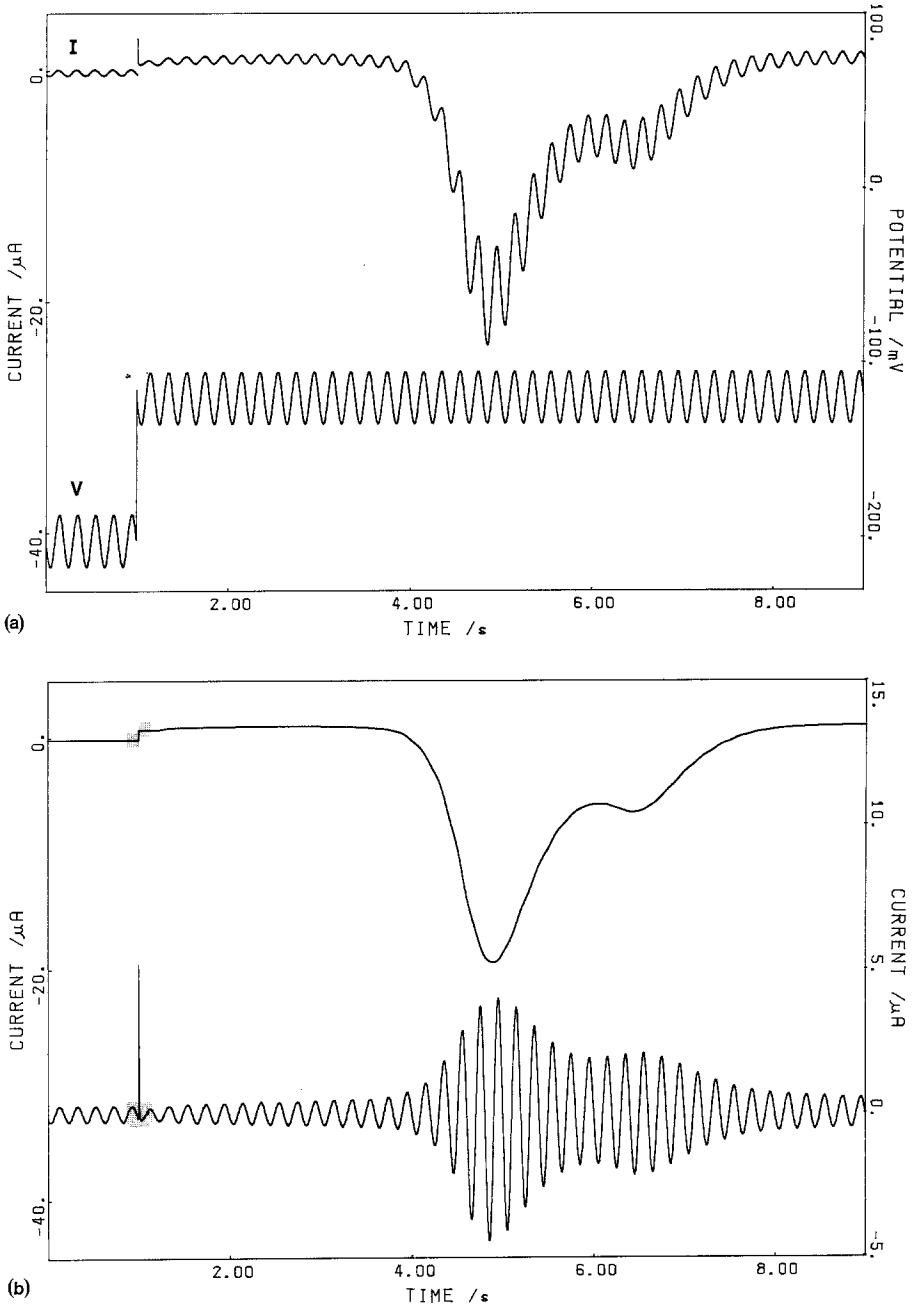

Fig. 4. (*a*): A cell response (upper trace) to a clamp potential (lower trace) incorporating the 5-Hz sine wave. The total clamp run took 16 sec. (as in Fig. 2), but only 9 sec is shown. (*b*): The current baseline (upper curve) and the current sine wave (lower trace) produced by the program STRIP. The shaded regions represent the extrapolated parts of the curves (*see* Methods). Similar regions can be found as the clamp level changes back to the resting potential

tached to TEST4. (The input offset voltage of the voltage follower being less than the A/D accuracy.) The conversion factors for the combination of *A*3 and *I*2 and for *I*1 were measured with *S*1 closed and stored on disk for use in all calculations.

To calibrate the clamp current arm (i.e., *A*4 and *I*3), *S*2 was opened and a known current source (a mercury cell with a series of accurate resistors) was attached at TEST5. The current measured by the A/D was plotted against the known input values. The amplification factors and offsets were calculated and stored on disk.

This calibration program was built into the COMSET program and was usually run before and after an experiment.

The above procedure ensured an accurate measurement of both the potential sinewave amplitude V_o and the current sinewave amplitude I_o, thus providing the magnitude of the admittance vector, Y_o. To obtain the phase angle ϕ due to the membrane reactance, two corrections had to be applied to the measured phase angle: a skew error $\Delta\phi_{A/D}$ and a response error $\Delta\phi_{clamp}$.

The skew error arose as only one A/D was available and the clamp current and the clamp potential were sampled consecutively. $\Delta\phi_{A/D}$ depended on the sampling rate and could be expressed as:

$(3/8) \times (2\pi/\text{number of sampling steps per cycle})$.

The correction was obtained by substracting $\Delta\phi_{A/D}$ from the measured phase angle.

$\Delta\phi_{clamp}$ was caused by the finite time necessary for the comparator and the various amplifier stages to respond. The error was evaluated by voltage clamping known resistors in

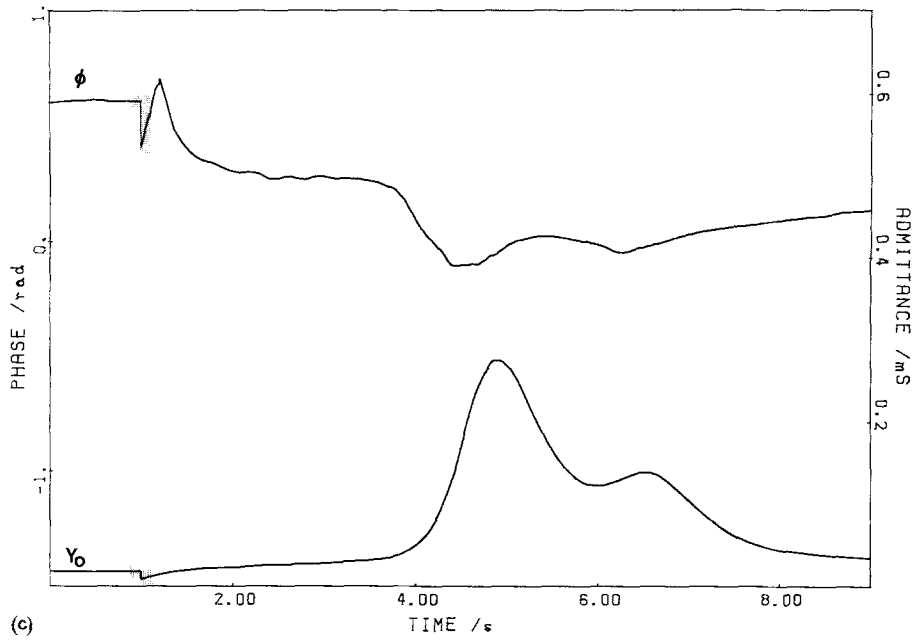

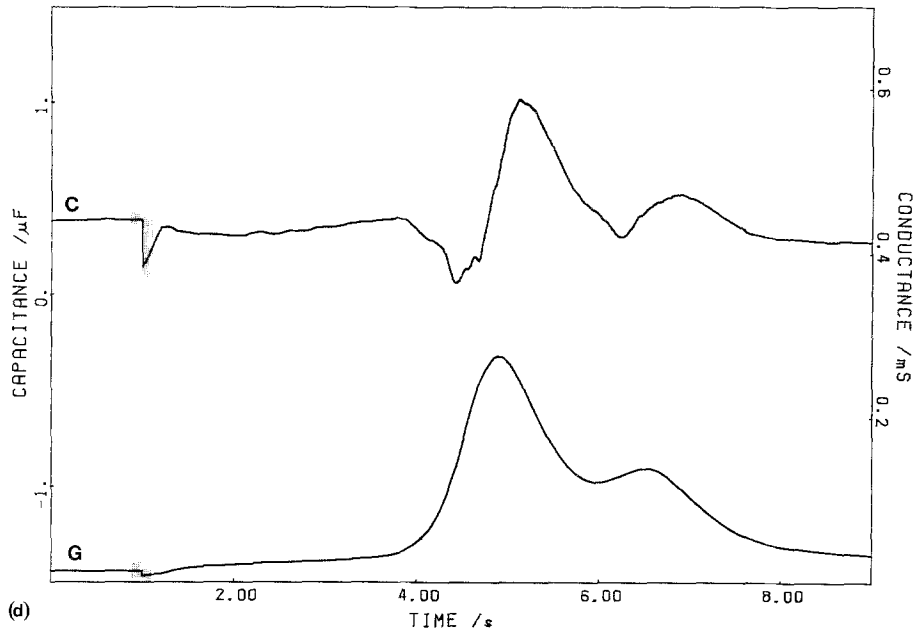

Fig. 4. (*c*): The phase angle ϕ (upper trace) and the admittance magnitude Y_o (lower trace). (*d*): The capacitance (upper trace) and the conductance (lower trace). The cell area was 17 mm^2

a range 200–500 k Ω. $\Delta\phi_{\text{clamp}}$ remained relatively constant for $R > 1$ k Ω.

The total absolute error in ϕ, $\Delta\phi$, was found to be ± 0.003 radians. This rather large error was mainly caused by a drift in $\Delta\phi_{\text{clamp}}$. We hope to improve our accuracy in the future by experimenting with different designs of the comparator *A*2 and the current amplifier *A*4.

To test the accuracy of the apparatus, the cell was replaced by a parallel *RC* circuit. The potential-measuring electrodes *E*1 and *E*2 were simulated by 10 M Ω resistors. The resistance could be measured within 2% for $500\ \Omega < R < 500$ k Ω. The accuracy of the *R* measurement was not greatly affected by large $\Delta\phi$. For small phase angles *R* was almost independent of ϕ. As ϕ increased and became more important in the calculation of *R*, ϕ could be measured more accurately.

The apparatus was thus tested over a wide range of *RC* values using program SINUS. As expected, the value of the measured capacitance was strongly dependent on the phase angle and consequently on the magnitude of *R*. Figure 6 shows measurements of *C* in the range 0.01 μF to 1 μF for different values of *R*. The error in *C* was calculated from Eq. (7):

$$\Delta C/C = \Delta Y_o/Y_o + \Delta\phi/\tan\phi \tag{8}$$

where $\Delta Y_o/Y_o$ was taken as 2%. The calculated absolute error, ΔC, is shown in Fig. 6 for two values of *R*. The actual measurements seem to indicate, however, that the estimate of $\Delta\phi$ was too pessimistic. As the accuracy of the resistance measurement was found to be virtually independent of the *C* in parallel, it was possible to put confidence limits on all the *C* measurements.

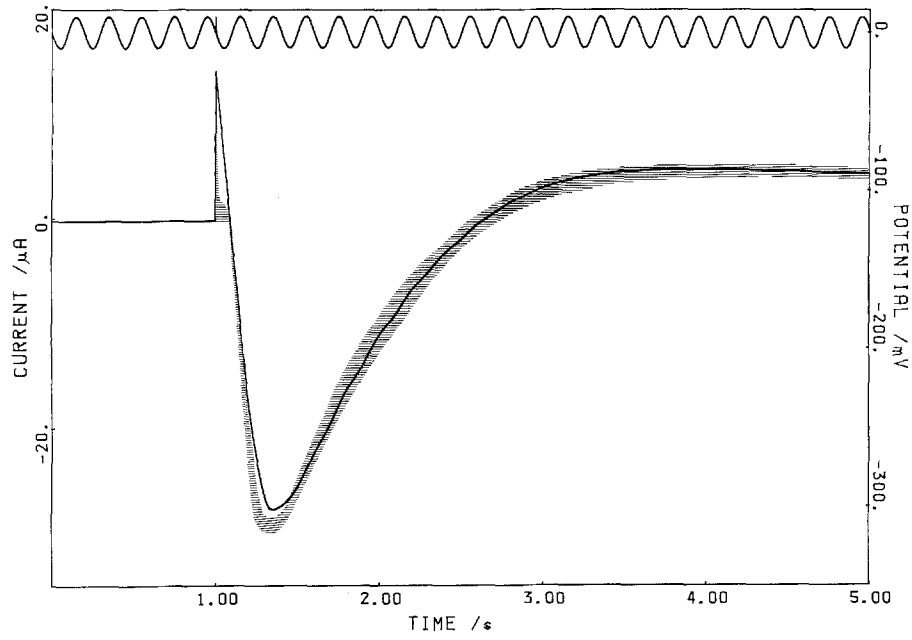

Fig. 5. Clamp current baseline at −80 mV (solid line) compared with four unmodulated clamp currents at the same potential level (shaded region). The potential sine wave (upper trace) is included for reference purposes. The cell area was 17 mm^2

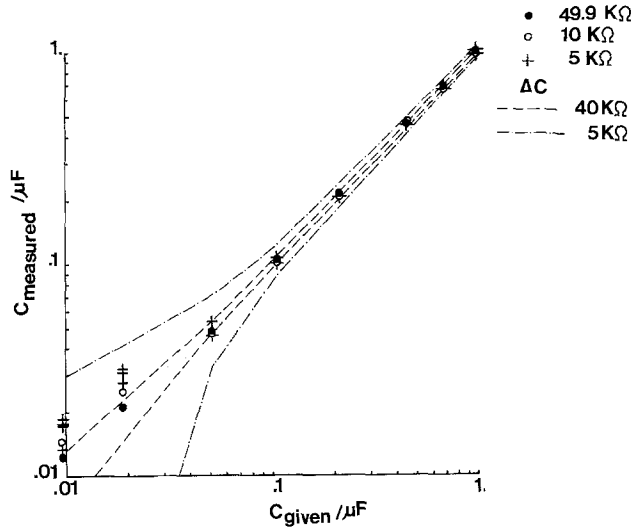

Fig. 6. Calibration of the capacitance measurement. Experimental C readings (y axis) are plotted against the known values (obtained with Wayne-Kerr bridge). The absolute error, ΔC (calculated from Eq. (8)), is shown for parallel resistances of 40 and 5 kΩ (representing a typical total resting resistance and total resistance at excitation peak, respectively) as various broken lines

Results

Steady-State Admittance

The admittance of 5 Hz, $Y(5)$, was measured for potentials ranging from 0 to −400 mV. This potential interval was delimited by punchthrough at the negative end and rectification at the positive potentials. Both these phenomena involve high conductance and the cell membrane is damaged if the above potential values are exceeded. In the excitable region the transients have been allowed to decay, before the admittance was calculated (*see* Materials and Methods). The angle ϕ and the admittance magnitude Y_o are shown in Fig. 7*a* and *b*, respectively. Y_o showed a large SE (standard error) for points more positive than −100 mV, thus reflecting the varying degrees of membrane rectification in different cells. The phase angle ϕ exhibited relatively constant SE throughout the potential range.

The solid line in Fig. 7*b* is the polynomial of the best fit to Y_o $(=I_o/V_o)$. The broken line is the polynomial fitted to G $[=(I_o/_o)\cos\phi]$ calculated from the same data. Both Y_o (5) and G (5) exhibit a central maximum at ~ −250 mV.

The capacitance was calculated using Eq. (7) and can be seen in Fig. 8. The capacitance showed no definite trend, although there might be a small dip at −120 mV and at −350 mV. Above −50 mV, ϕ is very small and results are unreliable (at 0 ϕ becomes negative and C should also become negative). The scatter in C was large. This was not only due to the variation from cell to cell, but also to the drift with time in a single cell (e.g., in cell 6 the resting C at the start of the experiment was 0.025 Fm^{-2}, at the end of the experiment it had decreased to 0.0139 Fm^{-2}).

The DC admittance, which becomes the conductance, G_s (0), was obtained with the staircase clamp command (*see* Methods). As the staircase pulses were short (*see* Fig. 3*b*), G_s (0) in the excitable region was measured before excitation occurred. The potential range was limited to −400 to −50 mV, as above −50 mV the delay before

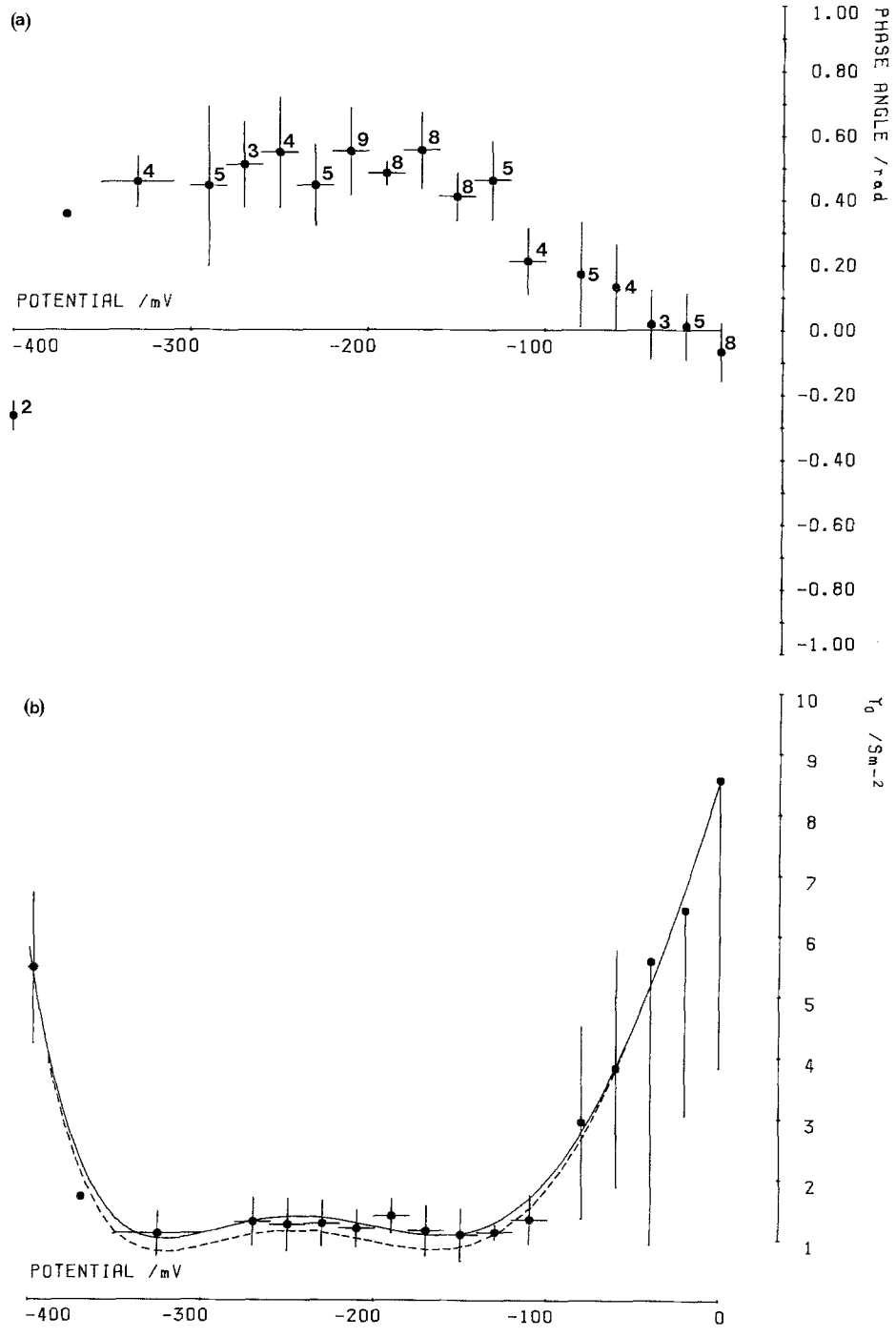

Fig. 7. (*a*): The phase angle ϕ. The data were gathered from seven cells. Some clamp levels were repeated. The numerals next to each point refer to number of clamp runs. The vertical bars are the SE; the horizontal bars indicate the groupings of data points within that potential interval. (*b*): The admittance amplitude Y_o. The solid line is the polynomial of the best fit. The broken line is the polynomial of the best fit the conductance data. (The conductance was calculated from Eq. (6)). Data has been processed as in *a*

excitation became too short (Beilby & Coster, 1979*b*) and the transients were triggered even by the short pulses. A polynomial was fitted to the V/I curve (Fig. 9*a*) and $G_s(0)$ was obtained as dI/dV (Fig. 9*b*). $G_s(0)$ showed a central maximum similar to that of $G(5)$. $G_s(0)$ has been calculated for eight cells. All showed the central maximum. The position of this feature varied between -120 and -250 mV, the amplitude from 0.1 Sm^{-2} to 2 Sm^{-2}.

The DC conductance at long times, $G_l(0)$, was also measured. The current baselines at the end of the clamp to various levels (between 12 and 13 sec) were plotted against clamp potentials (Fig. 9*c*) and the same procedure was applied as with the staircase V/I curves (*see* Fig. 9*d*). Note the different current scale in Fig. 9c. As the data were gathered over several hours, there was more scatter than in the "instantaneous" V/I curve and the conductance calculation was less accurate. The

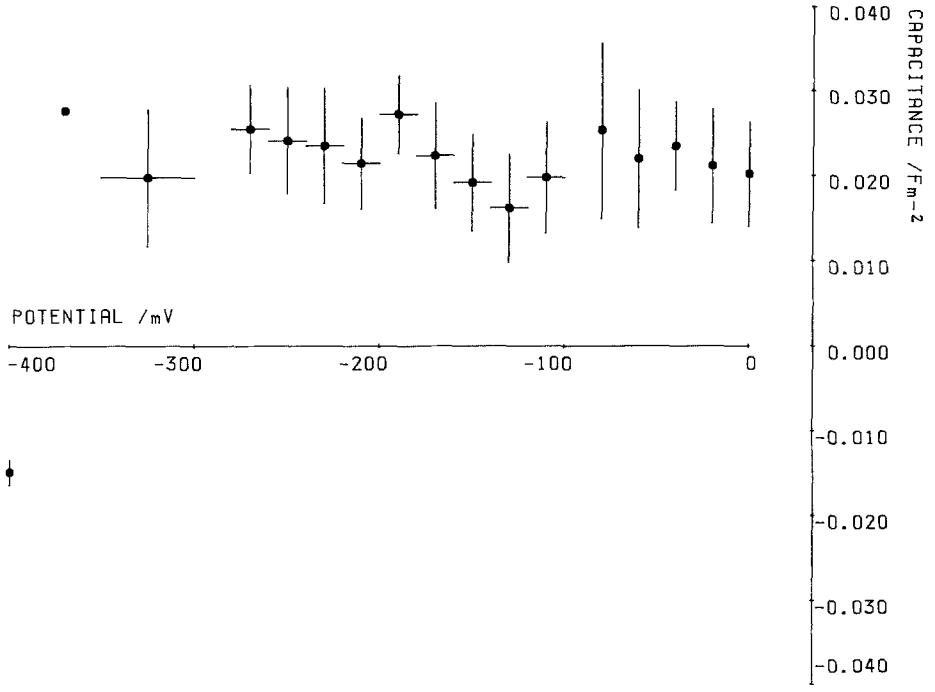

Fig. 8. The capacitance (calculated from Eq. (7)) at 5 Hz as a function of clamp potential. Data processing as in Fig. 7

central maximum was again present, but in this case it could be an artifact of the scatter. In the punchthrough region G_l (0) rose faster than both G_s (0) and G (5). In the first instance this behavior was expected, as the time-dependence of punchthrough is well documented (e.g., Beilby & Coster, 1976). Since G (5) was measured at the same stage of the clamp as G_l (0), the results of the second comparison was surprising. However, the data were sparse; G (5) at -400 mV was an average of conductances of cells 6 and 12, while G_l (0) was calculated from cell 12. A more detailed study is necessary.

A direct comparison of G_s (0) (continuous line) and G (5) (points) in Fig. 9*b* reveals similar profiles, but shifted with respect to each other by 25 to 50 mV. Both sets of results were obtained from cell 12. It will be interesting to investigate the reproducibility and frequency-dependence of the conductance profiles.

Excitation Admittance

The admittance at 5 Hz was also recorded at the time of excitation. The most reliable results were obtained at potentials more negative than -80 mV (*see* Methods). The phase angle ϕ and Y_o can be seen in Fig. 4*c* for a clamp potential for -120 mV. The conductance and capacitance are shown in Fig. 4c. The changes in G follow the changes in the baseline current closely (*see* Fig. 10, *also compare* Fig. 4*b* and *d*). Figure 10 also shows that during the delay (before excitation commences) the conductance was lower than after excitation.

The capacitance showed only a small change upon the shift of the clamp potential from the resting level to -120 mV (*see* Fig. *d*). As the conductance rose sharply, the capacitance decreased, but later rapidly increased reaching a maximum ~ 0.2 sec after the conductance peak. The second peak of the conductance was also echoed by the capacitance with a similar delay.

The behavior of C and G over the excitable potential region is summarized in Fig. 11*a* and *b*. The data were compiled from cell 6. The capacitance maxima (up to 0.1 Fm^{-2}) seem approximately proportional to the increase in G and thus to the amount of charge transferred (as G follows I closely).

Admittance at Punchthrough

The punchthrough phenomenon (e.g., Coster, 1965) was not investigated thoroughly here. It seems, however, that at the time of punchthrough, the capacitance becomes negative (*see* Fig. 12). The conductance and the current followed different time-courses. G remained high as the potential was returned to the resting level (*see* Fig. 12).

Discussion

Steady State

The resting potential values of G (5), 1.2 Sm^{-2}, and C (5), 0.022 Fm^{-2}, respectively, are in good

agreement with Coster and Smith (1977) measurements for the *Chara* plasmalemma. Also the similarity of the magnitudes of $G(0)$ (Fig. 9*b* and *d*) and $G(5)$ (Fig. 7*b*) is consistent with their observation that G as a function of frequency flattens out below 5 Hz.

The central maximum in the profiles of $G(5)$, $G_s(0)$, and perhaps $G_l(0)$, has not been observed before in *Chara*. This is rather surprising, especially for $G_s(0)$, as the staircase method was used extensively (e.g., Walker et al., 1979; Bisson & Walker, 1980; Smith & Walker, 1981). While the differentiation of a polynomial of the best fit is a procedure fraught with artifacts, the existence of the central maximum was confirmed by the 5 Hz measurements (*see* Fig. 9*b*).

It seems likely that the central maximum in the G profiles reflects tha G/V characteristics of the H^+ pump. APW of pH 7.5 was used throughout all experiments and most of the cells investigated exhibited the "hyperpolarized state," which is attributed to the action of the H^+ pump (e.g., Spanswick, 1972, 1981; Richards & Hope, 1974; Walker, 1982). It has been reported previously that the hyperpolarized state can be inhibited in media of low pH (Richards & Hope, 1974), without added Ca^{++} (Hope & Walker, 1961) or temporarily by an action potential (e.g., Spanswick, 1972; Bisson & Walker, 1981). In our experiments the potential is controlled by the voltage clamp. It could be reasoned that the conductance of the pump may decline if the potential is held at depolarized levels above -100 mV. Smith and Beilby (1983) quantified the temporary conductance decrease after the action potential as $\sim 1\ Sm^{-2}$. Assuming G (pump) to be negligible at potentials > -100 mV, the amplitude of the central maximum is of similar magnitude (*see* Results). This line of thought would indicate that the pump response to the potential change is rapid, as the staircase pulses are only ~ 30 msec wide. Thus for most potential levels in the excitable region the pump would not contribute to the membrane conductance contrary to models proposed by Kishimoto, Kami-ike and Takeuchi (1980) and Keifer and Lucas (1982).

For conclusive proof a systematic study of the central maximum of the G/V curves will be necessary at a range of outside pH, with inhibitors and after excitation. Hopefully, these measurements may reveal the potential dependence of the *Chara* H^+ pump.

The comparison between G and admittance magnitude (Fig. 7*a*) indicates that the "true" conductance $[(I_o/V_o)\cos\phi]$ can be up to 30% smaller than I_o/V_o. This difference is proportional to the phase angle ϕ, which is at maximum in the resting potential region (Fig. 7*a*). Above -100 mV and below -350 mV, ϕ becomes small and G tends to I_o/V_o.

The capacitance figures exhibit a rather large SE (Fig. 8). The origin of this variability is not yet known. One possibility is a formation and/or redistribution of acid and alkaline bands at the cell surface. Chilcott et al. (*see* footnote 1) found that the capacitance in the alkaline zone is somewhat smaller than that in the acid region. (Our use of the longitudinal current-injecting electrode averages Y_o and ϕ over the whole cell). However, the zones of different pH at *Chara* surface also strongly affect the conductance, and the scatter there was smaller, apart from the punchthrough and rectifying regions. Further, we use very young cells with little or no $CaCO_3$ deposits. The banding patterns in such cells have been little explored at present. To abolish any possible banding, the experiments should be repeated with the cell in the dark (J.R. Smith, *personal communication*).

The Double Fixed Charge Membrane (DFCM) theory constructs a mathematical model of two regions of opposite charge in contact with each other (Coster, 1965). This model successfully explains the rectification, punchthrough and G, C frequency dispersion (e.g., Coster, 1965, 1973). DFCM also predicts that the capacitance will almost triple as the potential across the membrane changes from -350 mV to 0 (Coster, George & Simons, 1969). An increase in capacitance with depolarization was, indeed, found in the axon (Takashima, 1976), but our capacitance data show no over-all trend in this potential range. A version of the DFCM model was proposed by Adam (1970), where a neutral region was interposed between the two fixed charge regions (psn-junction). In this model C is insensitive to membrane potential. The psn-junction, however, does not display the punchthrough behavior. Thus either version of the fixed charge model cannot explain our present capacitance data[2].

Excitation

The changes in the conductance at the time of excitation are of similar magnitude as observed by Findlay and Hope (1964) (The phase angle de-

[2] Our experimental data need not invalidate the applicability of the DFCM model to bio-membranes, as it is probable, that only some of the protein modules in the membrane are of the DFCM type. Their contribution to the admittance of the membrane only becomes important in the punchthrough and rectifying regions (H.G.L. Coster, *personal communication*)

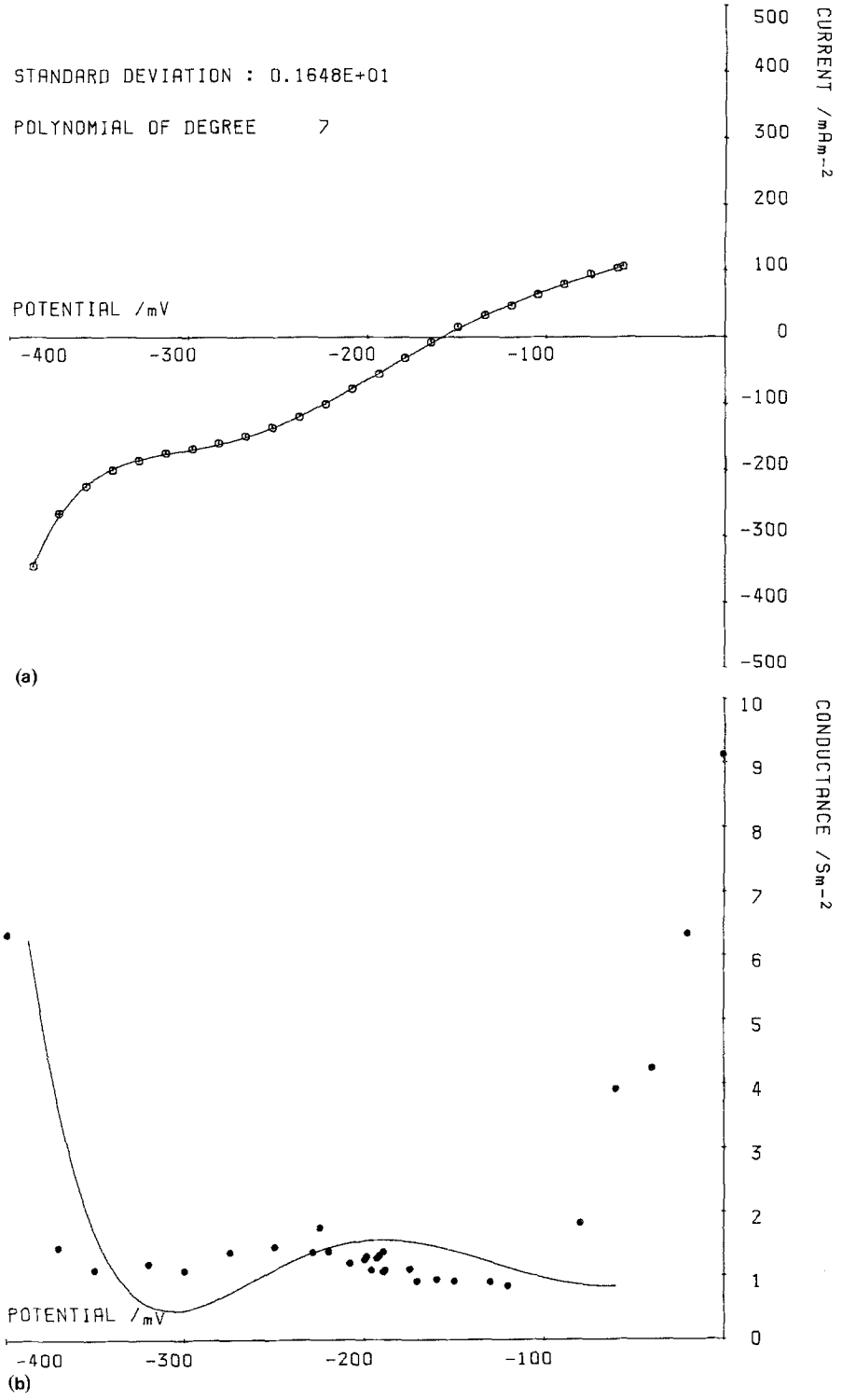

Fig. 9. (*a*): *V/I* curve generated by the program VIPLOT from the staircase data of Fig. 3 (points). The solid line is a polynomial of the best fit. (*b*): The slope conductance obtained by differentiation of the polynomial of the best fit in *a*. The measured conductance at 5 Hz has been included for comparison (points).

creases at the time of excitation (*see* Fig. 4*c*) and I_o/V_o is a good approximation for the conductance). The changes in G (5) were found to follow closely the baseline current (*see* Fig. 10). Invoking the Hodgkin-Huxley (HH) equations adapted to *Chara* (Hodgkin & Huxley, 1952; Beilby & Coster, 1979*b*), the total current at the time of the voltage clamp can be expressed as:

$$I_T = G_{Cl}(V - V_{Cl}) + G_{Ca}(V - V_{Ca}) + I_{ss} \quad (9)$$

G_{Cl} = conductance due to the Cl^- transient

G_{Ca} = conductance due to the Ca^{++} transient

I_{ss} = steady-state current

V_{Cl}, V_{Ca} = Nernst potentials for Cl^- and Ca^{++}, respectively.

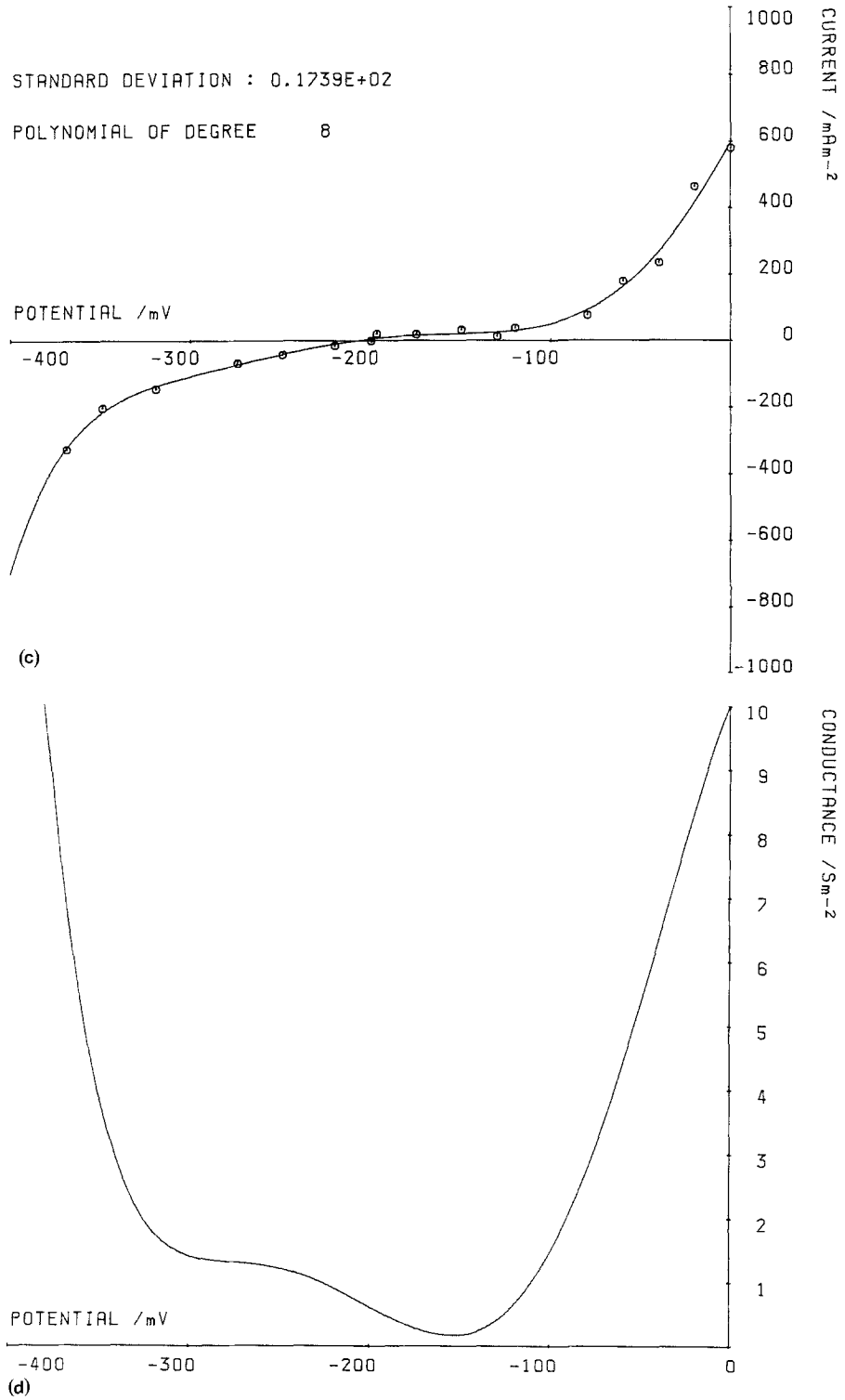

Fig. 9. (*c*): The current baselines at the end of each run (before reclamping to resting potential) were plotted against the clamp levels. A polynomial was again fitted and the long time DC conductance $G_l(0)$ obtained by differentiation (*d*). Note the different scale on the current axis. (*d*): Long time conductance obtained as in *b*

Near the threshold, the chloride and the calcium currents are fairly well separated, so that the first current peak can be approximated by the first and the last term in Eq. (9). As I_{ss} was defined as time-invariant (Beilby & Coster, 1979*b*) and V is controlled by the voltage clamp, I_T will be proportional to G_{Cl}, if V_{Cl} remains constant at the time of the clamp. This, indeed, seems to be case in Fig. 10, apart from the conductance rising slightly faster than the current. Similar behavior can be observed with the second peak with a different constant of proportionality $(V-V_{Ca})$.

At the time of the delay before excitation commences (*see* Figs. 10 and 4*d*), the conductance was lower than after excitation. This result challenges the findings of Beilby and Coster (1979*c*); the vari-

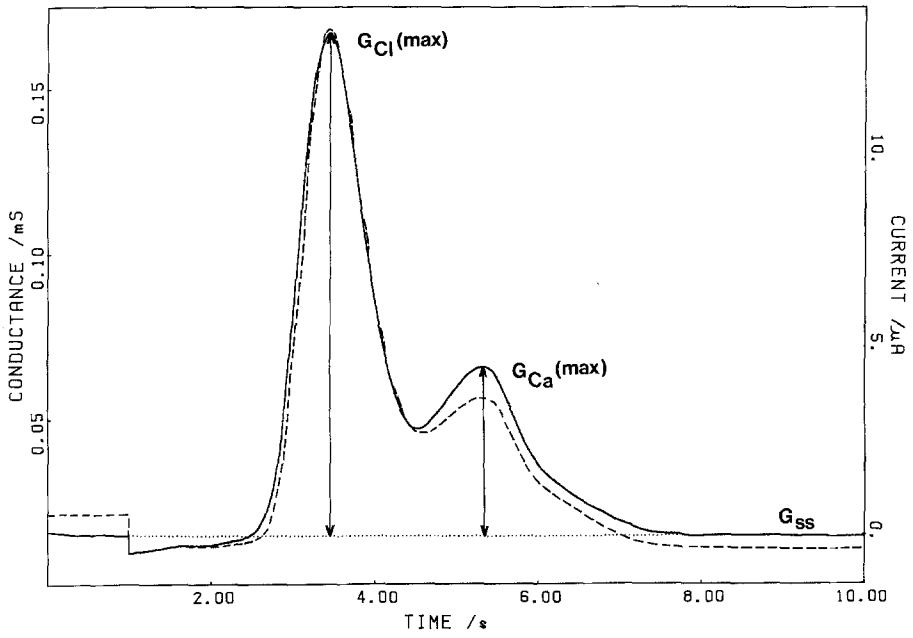

Fig. 10. A comparison between the inverted baseline current (broken line) and the conductance (solid line). The estimated (HH equations were not fitted) maximum amplitudes of G_{Cl} and G_{Ca} are also shown. The level of the steady-state conductance, G_{ss}, is marked by a dotted line. Note the low conductance at the time of the delay before excitation. The cell area was 17 mm^2

ation of the delays in Cl^- and Ca^{++} currents with temperature and potential indicated a transfer of charge across the membrane other than the ionic currents. Higher conductance was thus expected before excitation than afterwards. The delays will have to be investigated at a range of frequencies as the effect observed by Beilby and Coster may be only visible at particular frequencies.

The slow time scale of the *Chara* action potential is a mixed blessing: it allows a leisurely measurement (compared with the axon), but it also leaves enough time for the ionic profiles at the membrane/cell wall interfaces to change. Electrical effects arise, distracting from the membrane phenomena. Barry and Hope (1969*a*, *b*) drew attention to consequences of passing a current across a membrane which is selectively permeable to a given ionic species. In *Chara*, for instance, near the resting potential the permeability to K^+, P_K, is greater than the permeability to Cl^-, P_{Cl}. At the time of excitation, however, P_{Cl} increases above P_K. Such discontinuities in the transport numbers (Barry & Hope, 1969*a*) cause an enhancement and a depletion in the concentrations adjacent to the membrane when current flows across it. The build-up of ions induces a water flow across the membrane (local osmosis). Barry (1970*a*, *b*) measured such water flow at the time of the *Chara* action potential and found that it reached maximum $\sim$0.2 sec after the peak of the excitation. In the present study, the maximum capacitance increase also lags the peak of the excitation by $\sim$0.2 sec.

The excitation process increases the membrane permeability to Cl^- and Ca^{++}. The interfacial concentrations of K^+ and the above ions change due to the transport number effects. While the electroneutrality is preserved, there is a time-dependent decrease in the total membrane conductance. This conductance "creep" mimics capacitive effects (Barry, 1977, Smith, 1977). The fact that the increase in C is approximately proportional to the magnitude of the clamp current (as indicated in Fig. 11*a* by the amplitude of G_T, which was found to reflect I_T) fits with the finding of Barry and Hope (1969*b*), that the concentration build-ups are proportional to the magnitude of the current flowing across the membrane.

One set-back in this line of reasoning is the apparent invariance of V_{Cl} as indicated by application of Eq. (9). A further investigation is necessary.

The capacitance decrease at the time of the G rise does not seem readily explicable in terms of the transport number effects. Smith (1977) showed that the reactance due to the transport number effects could become inductive if the electro-osmotic coupling coefficient is large enough and the water flow sweeps away the external ionic concentrations in a manner that will enhance the conductance. It is difficult to explain, however, why the electro-osmotic coupling coefficient would change in the course of excitation.

The measurements of Cole and Curtis (1939) at high frequencies established the concept of the membrane capacitance as a passive quantity offering no information about the physiology of the membrane. However, later mathematical analysis

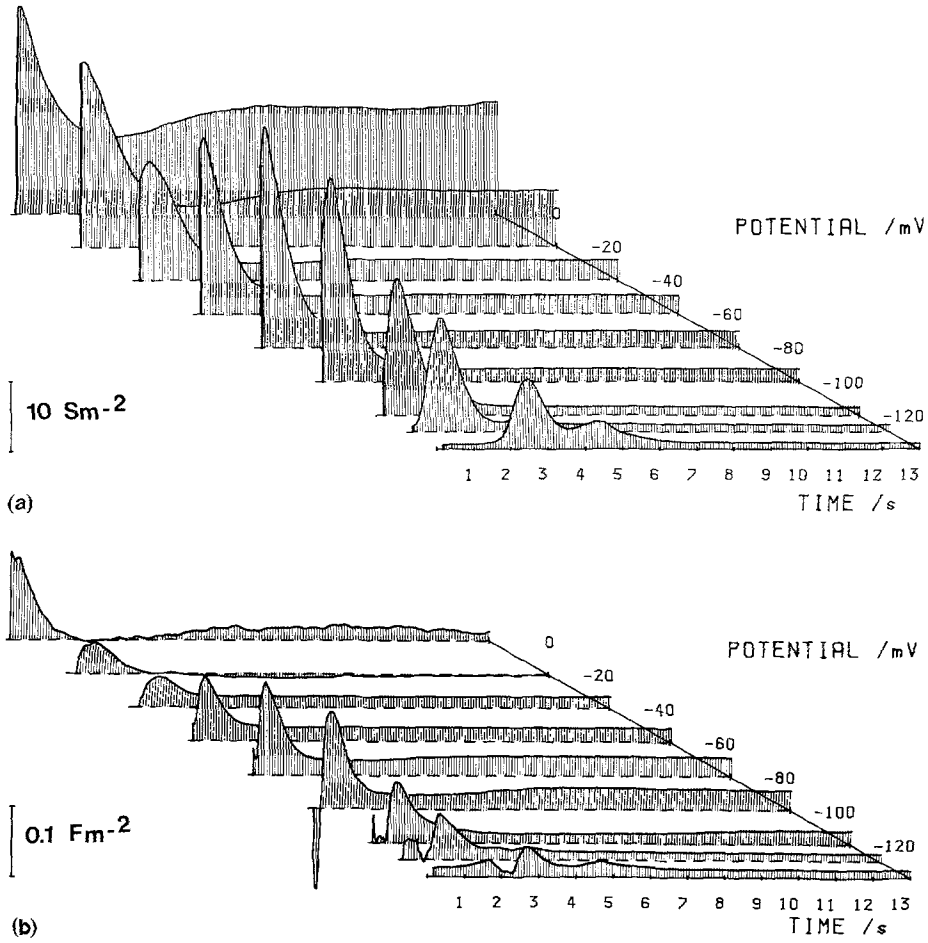

Fig. 11. The conductance (*a*) and capacitance (*b*) in the excitable potential region. The first 0.2 sec (one sine cycle) is not shown, as the results are unreliable (*see* Methods)

of Chandler et al. (1962) yielded an expression for admittance of the axon by linearizing the HH equations. The admittance includes reactive elements associated with the activation (m) and inactivation (h) processes. Further, recent measurements at low frequencies (e.g., Takashima, 1979) revealed capacitance changes at the time of the nerve action potential which has been slowed down by blocking the K^+ transient.

A preliminary calculation using HH parameters for *Chara* (Beilby & Coster, 1979*b*) indicated that the reactance associated with both m and h processes of the Cl^- transient is inductive. A quantitative estimate of the sizes of the inductance is difficult to obtain at present, as data on the long-time value of h, h_∞, is sparse in *Chara*. The magnitude of h_∞ is necessary in calculating the reactances for both the m and h parameters (e.g., Fishman, Pousart, Moore & Siebenga, 1977).

Smith and Coster (1980) suggested a method to distinguish between internal membrane phenomena and external concentration changes by observing the frequency dependence of the capacitance at different temperatures. The capacitance at the time of excitation can be tested in this fashion, when our apparatus is calibrated at a range of frequencies. Further, the transport number effects are relatively slow and their contribution to the total admittance of the system is thought to be negligible for alternating currents above 10 Hz (Barry, 1977; Smith, 1977). Thus experiments at higher frequencies should show the membrane admittance only.

Punchthrough

The different time courses of the membrane current and conductance (*see* Fig. 12) indicate that different processes are responsible for the massive Cl^- outflow (Coster & Hope, 1968), than in the action potential. The inductive nature of the reactance is not predicted by the DFCM theory.

The currents are large enough to produce substantial transport number effects. Beilby and Coster (1976) observed a depolarization in the resting potential following punchthrough, which indicates a change in the interfacial concentration of K^+. Barry and Hope (1969*b*) found a decrease

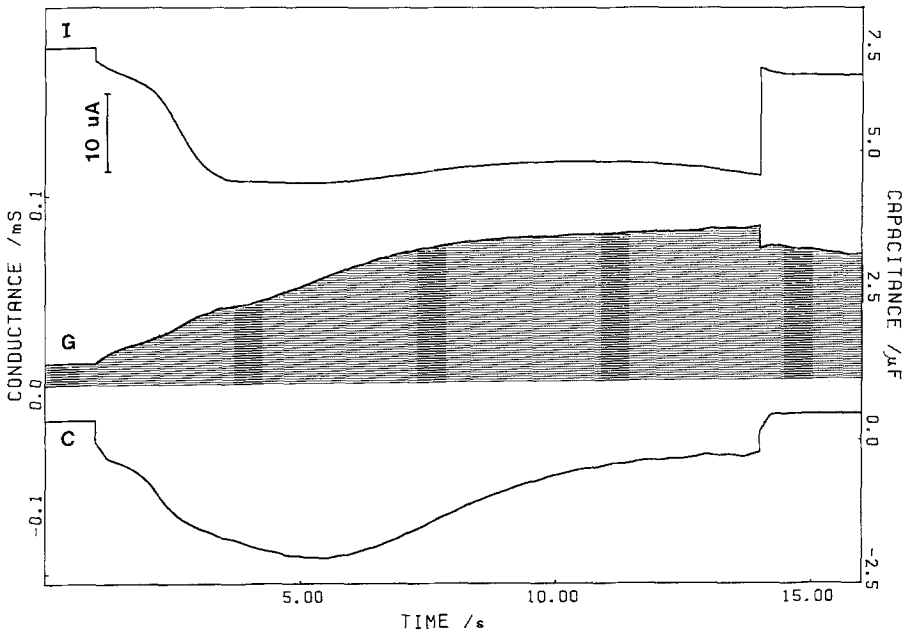

Fig. 12. The baseline current (top curve), conductance (shaded curve) and capacitance (bottom curve) at −400 mV, as the punchthrough occurs. The scale for the conductance is on the left, for the capacitance on the right. The current starts close to 0, as the potential is clamped at resting level for the first second. The scale is shown next to the current trace. The cell area was 17 mm^2

in volume flow at the time of punchthrough. It is not understood at present why the reactance is inductive at the punchthrough and capacitive at excitation.

Conclusions

1) DC conductance and conductance at 5 Hz display a maximum centered at ~ −250 mV, which has not been reported in *Chara* before. This feature may be attributed to the G/V characteristics of the H^+ pump.
2) The steady-state capacitance does not show any trend in the potential range −400 mV to 0, contrary to predictions of the DFCM theory.
3) At the time of excitation the conductance changes follow closely the time-course of the ionic currents.
4) At the time of delay before excitation commences, G (5) is smaller than after the excitation.
5) At the time of excitation the capacitance undergoes a sharp decrease followed by an increase.
6) At punchthrough the membrane becomes inductive.

Most of the above effects need further investigation, but it is apparent that the apparatus described is capable of providing varied and interesting data.

This work was done with support from the SERC, which is gratefully acknowledged.

We are indebted to Dr. E.A.C. MacRobbie for critical reading of the manuscript and to Assoc. Prof. N.A. Walker and Dr. J.R. Smith for helpful discussion.

References

Adam, G. 1970. Electrical characteristics of the ionic psn-junction as a model of the resting axon membrane. *J. Membrane Biol.* **3**:291–312

Armstrong, C.M., Bezanilla, F. 1973. Currents related to movement of the gating particles of the sodium channels. *Nature (London)* **242**:459–461

Barry, P.H. 1970*a*. Volume flows and pressure changes during an action potential in cells of *Chara australis*. I. Experimental results. *J. Membrane Biol.* **3**:313–334

Barry, P.H. 1970*b*. Volume flows and pressure changes during an action potential in cells of *Chara australis*. II. Theoretical considerations. *J. Membrane Biol.* **3**:335–371

Barry, P.H. 1977. Transport number effects in the transverse tubular system and their implications for low frequency impedance measurements of capacitance of skeletal muscle fibers. *J. Membrane Biol.* **34**:383–408

Barry, P.H., Hope, A.B. 1969*a*. Electroosmosis in membranes: Effects of unstirred layers and transport numbers. I. Theory. *Biophys. J.* **9**:700–727

Barry, P.H., Hope, A.B. 1969*b*. Electroosmosis in membranes: Effects of unstirred layers and transport numbers. II. Experimental. *Biophys. J.* **9**:729–757

Beilby, M.J. 1981. Excitation-revealed changes in the cytoplasmic Cl^- concentration in "Cl^--starved" *Chara* cells. *J. Membrane Biol.* **62**:207–218

Beilby, M.J., Coster, H.G.L. 1976. Effect of temperature on punchthrough in electrical characteristics of the plasmalemma of *Chara corallina*. *Aust. J. Plant Physiol.* **3**:819–26

Beilby, M.J., Coster, H.G.L. 1979*a*. The action potential in *Chara corallina*. II. Two activation-inactivation transients in voltage clamps of the plasmalemma. *Aust. J. Plant Physiol.* **6**:323–335

Beilby, M.J., Coster, H.G.L. 1979*b*. The action potential in *Chara corallina*. III. The Hodgkin-Huxley parameters for the plasmalemma. *Aust. J. Plant Physiol.* **6**:337–353

Beilby, M.J., Coster, H.G.L. 1979*c*. The action potential in *Chara corallina*. IV. Activation enthalpies of the Hodgkin-Huxley gates. *Aust. J. Plant Physiol.* **6**:355–365

Bell, D.J., Coster, H.G.L., Smith, J.R. 1975. A computer based, four-terminal impedance measuring system for low frequencies. *J. Phys. E.* **8**:66–70

Bisson, M.A., Walker, N.A. 1980. The *Chara* plasmalemma at high pH. Electrical measurements show rapid specific passive uniport of H^+ or OH^-. *J. Membrane Biol.* **56**:1–7

Bisson, M.A., Walker, N.A. 1981. The hyperpolarization of the *Chara* membrane at high pH: Effects of external potassium, internal pH, and DCCD. *J. Exp. Bot.* **32**:951–971

Chandler, W.K., FitzHugh, R., Cole, K.S. 1962. Theoretical stability properties of a space-clamped axon. *Biophys. J.* **2**:105–127

Cole, K.S. 1968. Membranes, Ions and Impulses. University of California Press; Berkeley

Cole, K.S., Curtis, H.J. 1939. Electrical impedance of the squid giant axon during activity. *J. Gen. Physiol.* **22**:649–670

Coster, H.G.L. 1965. A quantitative analysis of the voltage-current relationships of fixed charge membranes and the associated property of punchthrough. *Biophys. J.* **5**:669–686

Coster, H.G.L. 1973. The double fixed charge membrane. Low frequency dielectric dispersion. *Biophys. J.* **13**:118–132

Coster, H.G.L., George, E.P., Simons, R. 1969. The electrical characteristics of fixed charge membranes: Solution of the field equations. *Biophys. J.* **9**:666–684

Coster, H.G.L., Hope, A.B. 1968. Ionic relations of *Chara australis*. XI. Chloride fluxes. *Aust. J. Biol. Sci.* **21**:243–254

Coster, H.G.L., Smith, J.R. 1977. Low frequency impedance of *Chara corallina*: Simultaneous measurements of the separate plasmalemma and tonoplast capacitance and conductance. *Aust. J. Plant Physiol.* **4**:667–674

Curtis, H.J., Cole, K.S. 1937. Transverse electric impedance of *Nitella*. *J. Gen. Physiol.* **21**:189–201

Findlay, G.P., Hope, A.B. 1964. Ionic relations of cells of *Chara australis*. VII. The separate electrical characteristics of the plasmalemma and tonoplast. *Aust. J. Biol. Sci.* **17**:62–77

Fishman, H.M., Poussart, D.J.M., Moore, L.E., Siebenga, E. 1977. K^+ conduction description from the low frequency impedance and admittance of squid axon. *J. Membrane Biol.* **32**:255–290

Hodgkin, A.L., Huxley, A.F. 1952. A quantitative description of membrane current and its application to conduction and excitation in nerve. *J. Physiol. (London)* **117**:500–544

Hope, A.B., Walker, N.A. 1961. Ionic relations of cells of *Chara australis*. IV. Membrane potential differences and resistances. *Aust. J. Biol. Sci.* **14**:26–44

Keifer, D.W., Lucas, W.J. 1982. Potassium channels in *Chara corallina*. Control and interaction with the electrogenic H^+ pump. *Plant Physiol.* **69**:781–788

Keynes, R.D., Rojas, E. 1974. Kinetics and steady-state properties of the charged system controlling sodium conductance in the squid giant axons. *J. Physiol. (London)* **239**:393–434

Kishimoto, U. 1974. Transmembrane impedance of the *Chara* cell. *Jpn. J. Physiol.* **24**:403–417

Kishimoto, U., Kami-ike, N., Takeuchi, Y. 1980. The role of electrogenic pump in *Chara corallina*. *J. Membrane Biol.* **55**:149–156

Palti, Y., Adelman, W.J., Jr. 1969. Measurement of axonal membrane conductances and capacity by means of a varying potential control voltage clamp. *J. Membrane Biol.* **1**:431–458

Richards, J.L., Hope, A.B. 1974. The role of protons in determining membrane electrical characteristics in *Chara corallina*. *J. Membrane Biol.* **16**:121–144

Shimmen, T., Tazawa, M. 1980. Intracellular chloride and potassium ions in relation to excitability of *Chara* membrane. *J. Membrane Biol.* **55**:223–232

Smith, J.R. 1977. Electrical Characteristics of Biological Membranes in Different Environments. Ph.D. Thesis. pp. 65–80. University of New South Wales, Australia

Smith, J.R., Beilby, M.J. 1983. Inhibition of electrogenic transport associated with the action potential in *Chara*. *J. Membrane Biol.* **71**:131–140

Smith, J.R., Coster, H.G.L. 1980. Frequency dependence of the A.C. membrane impedance of *Chara*: The effect of temperature. *In*: Plant Membrane Transport: Current Conceptual Issues. R.M. Spanswick, W.J. Lucas, and J. Dainty, editors. pp. 609–610. Elsevier/North Holland, Amsterdam

Smith, P.T., Walker, N.A. 1981. Studies on the perfused plasmalemma of *Chara corallina:* I. Current-voltage curves: ATP and potassium dependence. *J. Membrane Biol.* **60**:223–239

Spanswick, R.M. 1972. Evidence for an electrogenic ion pump in *Nitella translucens*. II. Control of the light-stimulated component of the membrane potential. *Biochim. Biophys. Acta* **332**:387–398

Spanswick, R.M. 1981. Electrogenic ion pumps. *Annu. Rev. Plant Physiol.* **32**:267–289

Spear, D.J., Barr, J.K., Barr, C.E. 1969. Localisation of hydrogen ion and chloride ion fluxes in *Nitella*. *J. Gen. Physiol.* **54**:397–414

Takashima, S. 1976. Membrane capacity of squid giant axon during hyper- and depolarizations. *J. Membrane Biol.* **27**:21–39

Takashima, S. 1979. Admittance change of squid axon and during action potentials. Change in capacitive component due to sodium currents. *Biophys. J.* **26**:133–142

Walker, N.A. 1982. Membrane transport in charophyte plants: Chemiosmotic but electrically versatile. *In*: Membrane and Transport: A Critical Review. R. Martonosi, editor. Plenum, New York

Walker, N.A., Beilby, M.J., Smith, F.A. 1979. Amine uniport at the plasmalemma of charophyte cells: I. Current-voltage curves, saturation kinetics, and effects of unstirred layers. *J. Membrane Biol.* **49**:21–55

Received 28 September 1982; revised 16 December 1982